Electrochimica Acta 62 (2012) 263–268

Contents lists available at SciVerse ScienceDirect

Electrochimica Acta

journal homepage: www.elsevier.com/locate/electacta

Investigation of Au@Pt/C electro-catalysts for oxygen reduction reaction

Rui Lin[a,*], Haiyan Zhang[a,b], Tiantian Zhao[a], Chunhui Cao[a], Daijun Yang[a], Jianxin Ma[a,*]

[a] *Clean Energy Automotive Engineering Center & School of Automotive Studies, Tongji University, 4800 Cao'an Road, 201804 Shanghai, China*
[b] *School of Resource and Environmental Engineering, East China University of Science and Technology, Shanghai 200237, China*

ARTICLE INFO

Article history:
Received 1 November 2011
Received in revised form 6 December 2011
Accepted 8 December 2011
Available online 16 December 2011

Keywords:
PEMFC
Au@Pt/C electro-catalysts
Core shell nano-structure
MEA
ORR

ABSTRACT

Carbon-supported Au@Pt core shell nano-structured catalysts were synthesized by the seed-mediated growth method. The nano-structured catalysts were characterized by UV–vis spectroscopy, X-ray photoelectron spectra (XPS) and transmission electron microscopy (TEM) techniques. The oxygen reduction reaction (ORR) activity of the Au@Pt/C was tested by means of linear sweep voltammetry (LSV) by employing rotating disk electrode (RDE). It revealed that Au@Pt (2:4)/C (atomic ratio) catalyst exhibited the best catalytic activity toward ORR. Au@Pt (2:4)/C proceeded by an approximately four-electron pathway in acid solution, through which molecular oxygen was directly reduced to water. The stability of Au@Pt (2:4)/C is tested by cyclic voltammetry for 500 cycles. The performance of the membrane electrode assembly (MEA) prepared by Au@Pt (2:4)/C as the cathode catalyst in a single proton exchange membrane fuel cell (PEMFC) generated a maximum power density of 479 mW cm^{-2} at 0.431 V using H_2 and O_2 at 80 °C.

1. Introduction

Proton exchange membrane fuel cells (PEMFC), including direct methanol fuel cells (DMFC), have been recognized as environmentally friendly and highly efficient energy-converting devices. Critical issues still need to be solved before such cells can be commercialized for automotive applications. For example, the oxygen reduction reaction (ORR) is kinetically limited at the cathode [1], and the scale of the Pt crystallites leads to high costs for Pt-based electrocatalysts [2].

During the last decades, a number of strategies have been proposed for improving the performance of the electrocatalyst for the oxygen reduction reaction (ORR) and decreasing the cost of fuel cells. One way is to alloy Pt with other transition metals such as Fe, Co, Ni, and Cr [3]. Nevertheless, these alloy catalysts show poor long-term stability due to the dissolution of non-noble metals. Another approach is to develop Pt-free catalysts. Several promising candidates have been proposed in the past, such as oxides [4,5], carbides [6], Pd- [7], Ir- [8,9] and Ru-based binary catalysts [10], macrocycles (porphyrin or phthalocyanine), and non-precious catalysts [11,12]. However, until now these catalysts are not as good as Pt for ORR. In order to overcome these barriers, it is necessary to enhance the activity of Pt-based catalysts by optimizing morphology and/or composition.

Recently, core shell structure catalysts [13–16] have attracted intense attention owing to their shape-dependent properties. Their nano-architectures, compositions, and particle sizes can be easily adjusted in a controllable way to tune their magnetic, optical, electrical, and catalytic properties. Through that we can improve the utilization of Pt and then to reduce the cost of fuel cells. Furthermore, compared to single component Pt, Au@Pt and Pt@Pd core shell structured nano-particles show enhanced CO tolerance for hydrogen activation as well as higher activity toward oxygen reduction reaction [13]. In the groups of Xia and co-workers [14], it was reported that Pd–Pt bimetallic nanodendrites showed higher activity toward ORR which owed to the reasonably high surface area intrinsic to the dendritic morphology and the exposure of particularly active faces on the Pt branches. In the work of Adzic and co-workers [15], the mass specific activity of Pt sub-monolayer deposited on Ru or Au nanoparticles was found to be significantly higher than that of Pt particles for electro-catalytic O_2 reduction. In the work of Lee and co-workers [16], the CO anodic stripping peaks of the Au@Pt/C catalyst were all negatively shifted compared with a conventionally prepared Pt/C catalyst and Au@Pt/C catalyst which also promoted the methanol oxidation reaction.

There are normally two approaches to synthesize Pt–Au bimetallic nano-particles: successive or simultaneous reduction of the metallic precursors [16]. The successive reduction approach normally gives better controlling of the shape and atomic ratio compared to that of the simultaneous approach, and the synthesized Pt–Au nano-particles show core shell structures.

In the present study, we synthesized Au@Pt/C catalysts with controllable composition by successive reduction approach

---

* Corresponding authors. Tel.: +86 21 69589480; fax: +86 21 69589480.
E-mail addresses: ruilin@tongji.edu.cn (R. Lin), jxma@tongji.edu.cn (J. Ma).

0013-4686/$ – see front matter © 2011 Elsevier Ltd. All rights reserved.
doi:10.1016/j.electacta.2011.12.018

namely seed-mediated growth method. The resultant catalysts were characterized by UV–vis, X-ray photoelectron spectra (XPS) and transmission electron microscopy (TEM) techniques. The as-synthesized Au@Pt/C catalysts were investigated for oxygen reduction and compared with the commercial Pt/C (JM).

2. Experimental

2.1. Materials and catalyst synthesis

Chlorauric acid ($HAuCl_4{\cdot}4H_2O$), trisodium citrate dehydrate ($C_6H_5Na_3O_7{\cdot}2H_2O$), sodium borohydride ($NaBH_4$), chloroplatinic acid ($H_2PtCl_6{\cdot}6H_2O$) and ascorbic acid ($C_6H_8O_6$) were purchased from Sinopharm Chemical Reagent Company. Polyvinyl alcohol (PVA, repeating units 1750) was purchased from Aldrich Company. 5 wt% Nafion solution was from DuPont Company. All chemicals were analytical grade and were used as received.

Seed-mediated growth method was used to obtain Au@Pt nano-particles with the core shell structure. Citrate-stabilized Au nano-particles were prepared from $NaBH_4$ reduction of $HAuCl_4{\cdot}4H_2O$. Briefly, 1 mL of 48.5 mM aqueous $HAuCl_4{\cdot}4H_2O$ solution was mixed with 1 mL of 10 mg mL^{-1} PVA solution which was used as stabilizer. 5 mL of 0.1 M aqueous $NaBH_4$ solution was then added dropwise under vigorous stirring, giving to a bright red Au hydrosol. The Au hydrosol was aged for 12 h to decompose residual $NaBH_4$ before it was used in subsequent steps. To prepare the core shell structured Au@Pt, a stoichiometric amount of $H_2PtCl_6{\cdot}6H_2O$ was added to the Au seeds hydrosol. Then, an excess amount of ascorbic acid was added to the above solution at room temperature under stirring. The obtained solution mixture changed from red to dark brown after 2 h, which indicated the successful formation of Pt nanoparticles.

The carbon-supported Au@Pt/C catalysts were prepared by mixing a desired amount of Vulcan XC-72 carbon black (BET surface area: 235 $m^2\,g^{-1}$) with hydrosols, followed by careful adjustment of the acidity of the solution to pH = 1.5 with 1 mol L^{-1} HCl. Then the suspension was refluxed for 2 h under vigorous stirring. The powers were separated by filtration and then washed intensively with deionized water. The washed powders were dried in a vacuum oven at 353 K for 8 h to obtain the Au@Pt/C catalysts.

2.2. Characterization of the catalyst

2.2.1. Physicochemical characterizations

The morphology of the colloidal particles or electrocatalysts was characterized by transmission electron microscopy using a JEM-2011 system operating at 200 kV. X-ray photoelectron spectroscopy measurements of Au@Pt/C catalysts were carried out on a PHI 5000 C ESCA instrument. The optical properties of Au and Au@Pt colloids were monitored on a Hitachi U-3310 dual beam spectrometer operated at a resolution of 0.5 nm. The colloidal solution samples were filled in a quartz cell of 1 cm light-path length and the light absorption spectra were given in reference to deionized water.

2.2.2. Electrochemical measurements

The activities of the as-synthesized Au@Pt/C and commercial Pt/C catalysts were determined by cyclic voltammetry using a potentiostat CHI 720 electrochemical analyzer (CH Corporation, USA). The electrode was fabricated as follows: Au@Pt/C catalyst (2 mg) was suspended in methanol/Nafion® solution (30:1 wt%; 1 mL) to prepare the catalyst ink. Then, two 5 μL portions of the ink were transferred to a clean glassy carbon (GC) disk electrode (6 mm diameter). The overall loading of the mixed catalyst was 2.8×10^{-5} g cm^{-2} for the apparent electrode area of the GC disk (0.283 cm^{-2}). For comparison, 40% Pt/C (Johnson Matthey, JM) was measured by the same procedures.

The Au@Pt/C catalysts were tested for their electrochemical ORR activities in a glass cell consisting of a three-electrode system in 0.5 M H_2SO_4 at 25 °C, which was saturated by pure nitrogen in order to expel oxygen from the solution. A saturated calomel electrode was used as a reference, and a platinum wire was used as the counter electrode. The measurements were carried out using a rotating disk electrode (RDE; Pine, 5908 Triangle Drive, Raleigh, NC) by linear sweep voltammetry (LSV) at 5 mV s^{-1}, at rotation speeds of 300, 600, 1200, 1800, and 2400 rpm, respectively, to determine the current density at room temperature in O_2 streams. The electrolyte was saturated with oxygen for 10 min before each ORR electrochemical measurement.

The stability of the Au@Pt (2:4)/C catalyst in a glass cell consisting of a three-electrode system was tested in 0.5 M H_2SO_4 at 25 °C, which was saturated by pure nitrogen in order to expel oxygen from the solution. The cyclic voltammetry was cycled for 500 cycles using a potentiostat CHI 720 electrochemical analyzer (CH Corporation, USA). A saturated calomel electrode was used as a reference, and a platinum wire was used as the counter electrode. The electrode was fabricated as the method used in testing the activities of as-synthesized Au@Pt/C and commercial Pt/C catalysts.

2.2.3. Single-cell performance measurement

Au@Pt (2:4)/C sample was evaluated as the cathode catalyst in a single PEMFC. A membrane electrode assembly (MEA) was fabricated by the following strategies: 40% Pt/C (JM) and Au@Pt (2:4)/C catalysts were respectively used as anode and cathode catalysts. The ink was prepared by mixing catalyst with a solution of 5 wt% Nafion (Dupont) and iso-propanol and then was sonicated for 4 h. The catalytic ink was sprayed directly onto the 212 Nafion membrane at 100 °C to form the catalyst layer, with a metal loading of 0.4 mg cm^{-2}. The ratio of catalyst to Nafion was 3:1. This was followed by simply physically placing gas diffusion layers (GDLs) (fabricated with carbon paper, Toray TGP-H-090) without the need for a hot-pressing process.

The single-cell (50 cm^2) test on the PEMFC was performed under steady-state conditions of the fuel cell. An electronic load (Sun-Fel200a, Sunrise Power) was used for discharging. The discharging curves were measured to test the effect of the catalyst on the performance of the fuel cell. The cell was operated at 80 °C and 0.1 MPa. The temperatures of H_2 and O_2 were controlled at 80 °C by means of a heating tape. O_2 and H_2 were 100% humidified at 80 °C. The flow rates of H_2 and O_2 were fixed at 500 and 300 mL min^{-1}, respectively.

3. Results and discussion

3.1. Characterization of Au@Pt/C catalysts

UV–vis is a surface sensitive tool for the characterization of Au and Au@Pt nanoparticles. Fig. 1 shows the UV–vis absorption of aqueous suspensions of Au hydrosol and Au@Pt hydrosol. The mass of Au in colloidal solutions was the same in all cases. It can be seen that pure Au nanoparticles exhibits an absorbance peak at 520 nm due to their surface plasmon resonance property originating from the collective oscillation of their conduction electrons in response to optical excitation. As the case of Au@Pt nanoparticles, the absorbance peak weakened and moved toward shorter wavelengths. These spectra clearly demonstrate that the surface of Au nanoparticles have been mostly covered with Pt.

Fig. 2 shows the XPS spectra of the Au@Pt/C samples with varying the ratio of Pt to Au. According to the standard XPS spectra [17], the binding energy (BE) positions for pure Pt and Au were at 70.9, 74.2 eV and 83.8, 87.4 eV respectively. For all of the as-prepared Au@Pt/C samples, the BEs of Pt which were at 71.5 and 74.2 eV were attributed to Pt (0). Compared with Pt (0) standard spectra, it

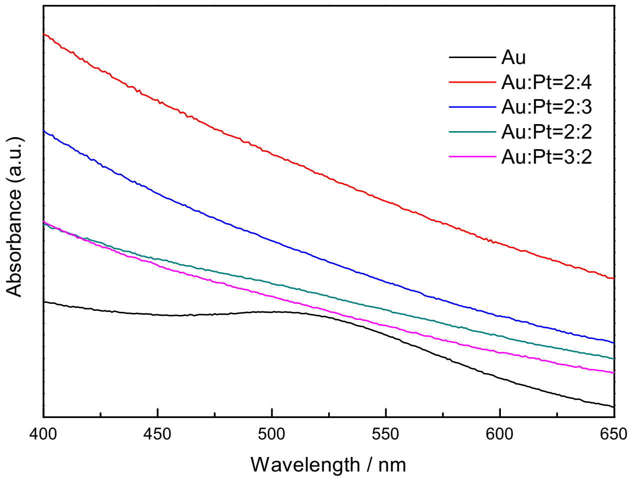

Fig. 1. UV–vis spectra of Au and Au@Pt hydrosol.

shifted to higher BE value. With reference to the signatures of the PtO and Pt(OH)$_2$ samples [18], these data suggested that some of Pt was in the phase of Pt (II) in the as-prepared Au@Pt/C samples. Nevertheless the BEs for Au (ca. 83.9, 87.4 eV) in the XPS spectra of Au@Pt/C particles did not shift in reference to pure Au, which could be taken as evidence for no formation of bimetallic alloy particles. Since Au–Pt alloys prepared by vapor deposition of Au on Pt substrate can lead to significant binding energy shift in XPS spectra [19]. Continued weakening of Au (0)4f signals was seen to accompany the appearance and strengthening of the Pt (0)4f signals. These results indicated that the surface of Au nanomaterials became covered by Pt with increasing the amount of deposited Pt in both synthetic systems, which was well consistent with the result of the UV–vis spectra.

Fig. 3 shows the TEM images of Au, Au@Pt hydrosol and Au@Pt/C electrocatalysts. Fig. 3a and b is respectively the TEM images of Au and Au@Pt (2:4) hydrosols. It is seen that the Au seeds are at about 2–3 nm in diameter, the Au@Pt (2:4) particles are at about 3–5 nm. From Fig. 3b, the core shell components of Au@Pt (4:2) are easily differentiable by TEM because of strong imaging contrast between Au and Pt. Fig. 3c–f is TEM images of Au@Pt (2:8)/C, Au@Pt (2:4)/C, Au@Pt (3:2)/C and Au@Pt (2:3)/C electrocatalysts. It is clearly seen that Au@Pt particles are well dispersed on the carbon support and the ratio of Pt to Au did not affect the particle size of Au@Pt. Only when the ratio of Au to Pt was over 2:4, Au@Pt (2:8)/C catalyst appeared to be partly aggregated. This suggests that the Au surface of Au@Pt/C (2:4) was completely covered with Pt over-layers. This superior structure and excellent dispersion of the metal nanoparticles might contribute to the superior adsorption and activation of oxygen molecules on the surface of Pt, hence the enhancement of the activity of the Au@Pt/C catalysts for oxygen reduction reactions, as will be discussed below.

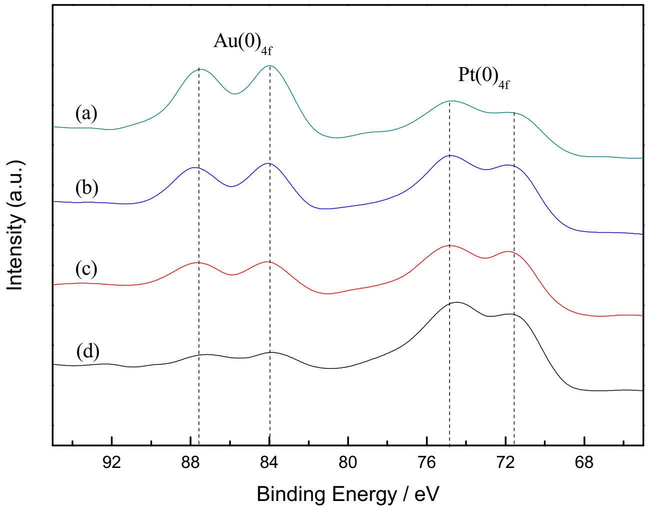

Fig. 2. XPS spectra of as-prepared Pt–Au/C samples: (a) Au@Pt (2:8)/C, (b) Au@Pt (2:4)/C, (c) Au@Pt (2:3)/C, and (d) Au@Pt (3:2)/C.

3.2. *Electrochemical performances*

In order to characterize the oxygen reduction activity in the electrolyte solution, we used herein the Au@Pt/C catalyst of different Pt/Au ratios and commercial Pt/C (JM) catalysts to demonstrate the change of LSV curves during the potential treatments in O$_2$-saturated 0.5 M H$_2$SO$_4$. The obtained voltammograms are shown in Fig. 4.

Fig. 4 indicates that ORR kinetics are not the same on all the catalysts. Oxygen reduction was facile in the case of Au:Pt at atomic ratios of 2:4 compared to that of Au:Pt at atomic ratios of 2:8, 2:3, 2:2 and 3:2. A high oxygen reduction current was paramount for an efficient electrochemical power device. In the case of Au@Pt (3:2)/C catalyst, the cathodic current commenced at 0.91 V and increased as the potential was scanned negatively to 0.05 V, whereupon no diffusion-controlled limiting current was observed due to the inferior catalytic activity of Au@Pt (3:2)/C. In the case of Au@Pt/C catalysts with Au:Pt atomic ratios of 2:8, 2:3 and 2:2, ORR was diffusion-controlled at potentials below +0.3 V and diffusion- and kinetics-controlled in the potential region between +0.3 V and +0.9 V vs. RHE. For the Au@Pt (2:4)/C catalyst, however, ORR was under diffusion control at potentials below +0.5 V and diffusion- and kinetics-controlled in the potential region between +0.5 V and +0.9 V vs. RHE, indicating the strong electrocatalytic activity toward ORR.

The limiting current densities are plotted as a function of the Au:Pt atomic ratios in Fig. 5. It shows that the current density exhibits a maximum value for the Au@Pt (2:4)/C catalyst. Further increasing the content of Au resulted in a decrease of the ORR activity. Recently Ma et al. [20] also observed the higher selectivity for oxygen reduction to water at moderate ratio (Au:Pt = 2:3) under cathode-relevant reaction conditions. Moreover, oxygen reduction activity of the as-synthesized Au@Pt (2:4)/C (4.0 mA cm^{-2}) was comparable to that of the commercial Pt/C (JM) catalyst (4.0 mA cm^{-2}) although the Pt content in Au@Pt (2:4)/C is 33% less than that in Pt/C (JM). This might be attributed to the improvement of the utilization of the Pt metal with the core shell structure. The interaction between the Au and Pt also might contribute to its high oxygen reduction. However from Fig. 4, in comparison with the Pt/C (JM) catalyst, the half-wave potential $E_{1/2}$ (the potential corresponding to one-half of the diffusion current) of Au@Pt (2:4)/C is negatively shifted by about 40 mV vs. RHE.

In order to investigate the kinetics of the ORR catalyzed by the Au@Pt/C catalyst, RDE measurements were carried out. Fig. 6 shows the ORR curves on Au@Pt (2:4)/C electro-catalyst in oxygen-saturated 0.5 mol L^{-1} H$_2$SO$_4$ solution at different rotating rates with a scan rate of 5 mV s^{-1}. The kinetics for oxygen reduction on the electrode was analyzed by Koutecký–Levich relationship. The reciprocal of the observed currents at 0.82 V on the RDE coated with Au@Pt (2:4)/C from Fig. 6 were plotted against the reciprocal of the square root of rotation rates, as shown in Fig. 7 in O$_2$ saturated 0.5 mol L^{-1} H$_2$SO$_4$ aqueous solution. From the following equations [21], the slope ($1/B$) is directly related to the total number of electrons (n) involved in oxygen reduction:

$$\frac{1}{i} = \frac{1}{i_k} + \frac{1}{B\omega^{1/2}}$$

$$B = 0.62nFAD_{O_2}{}^{2/3}\nu^{1/6}C_{O_2}$$

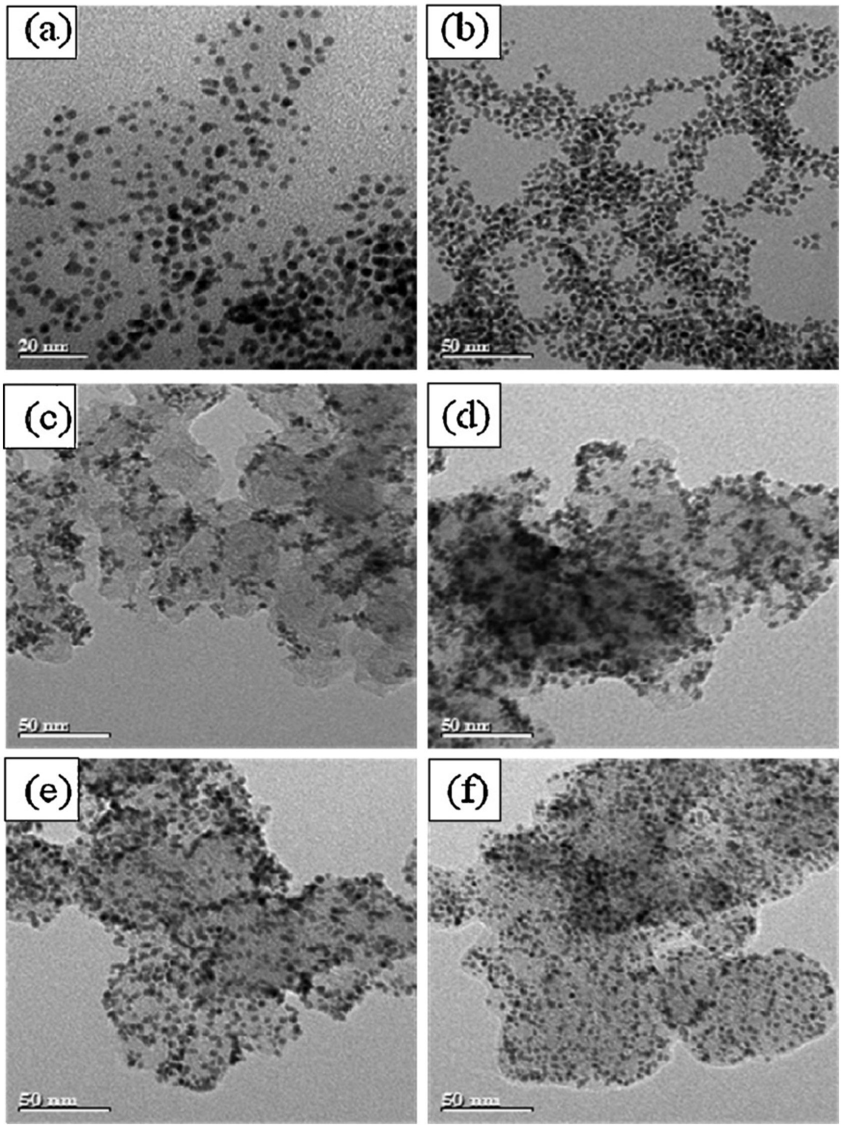

Fig. 3. TEM images of: (a) Au, (b) Au@Pt (2:4) hydrosol and (c) Au@Pt (2:8)/C, (d) Au@Pt (2:4)/C, (e) Au@Pt (2:3)/C, and (f) Au@Pt (3:2)/C electrocatalysts.

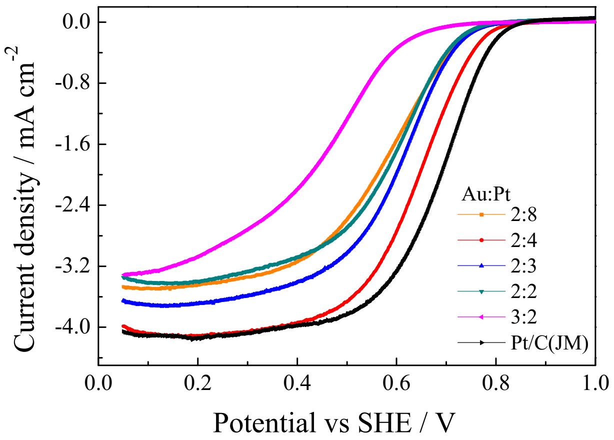

Fig. 4. Linear sweep voltammograms (LSVs) of O_2 reduction on Au@Pt/C and commercial Pt/C (JM) catalysts in O_2-saturated 0.5 M H_2SO_4 at room temperature. Sweep rate: 5 mV s^{-1}. Rotation speed: 1800 rpm.

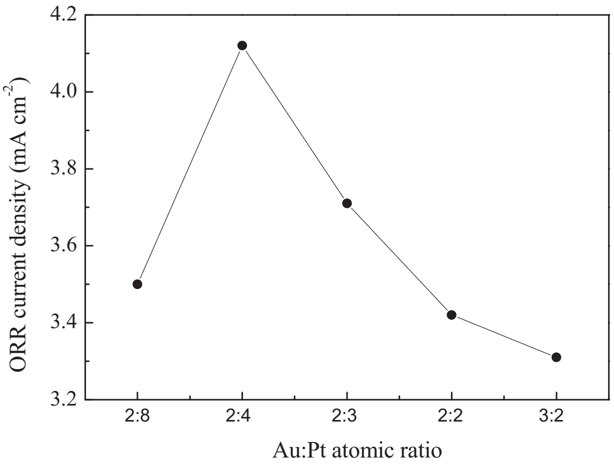

Fig. 5. Pt/Au atomic ratio vs. limiting current density of as-synthesized Au@Pt/C catalysts at 0.1 V from Fig. 4.

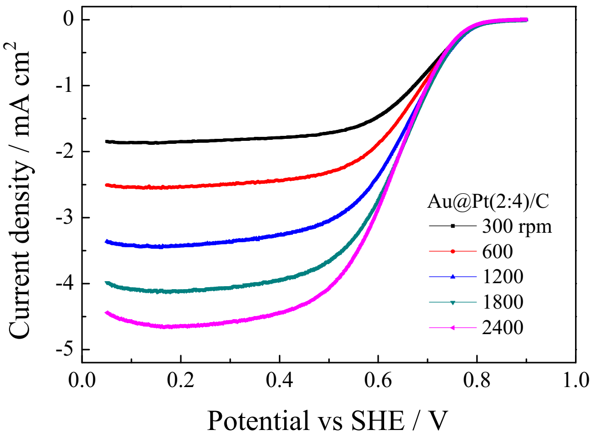

Fig. 6. RDE measurements for O_2 reduction on Au@Pt (2:4)/C in 0.5 M H_2SO_4 with different speeds of 300, 600, 1200, 1800 and 2400. Sweep rate: 5 mV s^{-1}.

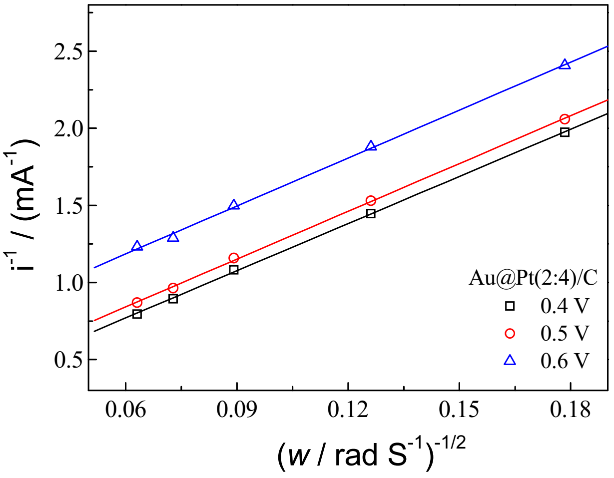

Fig. 7. Koutecký–Levich plots for O_2 reduction on Au@Pt (2:4)/C in 0.5 M H_2SO_4 derived from the data in Fig. 6.

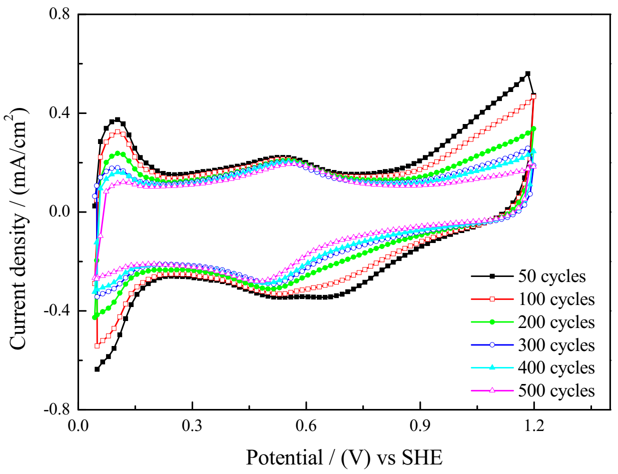

Fig. 8. The stability of the Au@Pt (2:4)/C catalyst in 0.5 M H_2SO_4. Sweep rate: 5 mV s^{-1}.

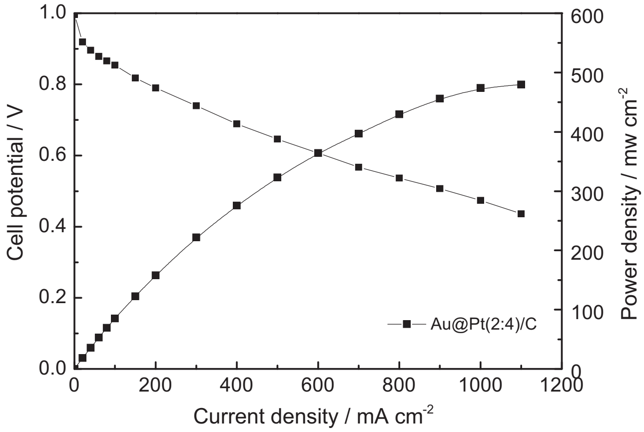

Fig. 9. Single-cell performances of Au@Pt (2:4)/C as cathode electrocatalyst.

where i is the experimentally observed current, i_k the kinetic current, n the number of electrons transferred per molecule of O_2 reduced, F the Faraday constant, A the electrode area, D_{O_2} the diffusion coefficient for oxygen, ω the rotation rate in rad s^{-1}, C_{O_2} the concentration of oxygen dissolved, and ν the kinematic viscosity of the sulfuric acid.

Table 1 shows the kinetic current (i_k) and average number of electrons transferred for O_2 reduction (n_i) on Au@Pt (2:4)/C at different potentials in 0.5 M H_2SO_4. It was found that the n value for the Au@Pt/C was derived to be 4.14–4.20 at the potential ranging from 0.4 to 0.6 V, indicating that an approximately four-electron process from oxygen to water for the ORR was on the Au@Pt/C electrocatalyst.

Au@Pt (2:4)/C catalyst was chosen to test the stability of the catalyst. The experiment was operated in 0.5 M H_2SO_4, at the scan rate of 0.05 V s^{-1} and cycled for 500 cycles. The results are showed in Fig. 8. It was found that the oxygen reduction and oxidation peaks reduced greatly after 100 cycles, but with increasing the cycles of CV curves, the change of the intensity of the oxygen reduction peaks is not obvious, especially the CV curves of 300 cycles are very close to that of 400 cycles, which indicates that the stability of this catalyst could be stable in certain period. But after 400 cycles, the peaks trend to reduce again.

Table 1
Kinetic current (i_k) and average number of electrons transferred for O_2 reduction (n_i) on Au@Pt (2:4)/C at different potentials in 0.5 M H_2SO_4.

i	E_i (V) vs. SHE	i_k (mA)	n_i
1	0.4	1.78	4.14
2	0.5	4.51	4.15
3	0.6	6.31	4.20

3.3. Single-cell performance

Fig. 9 shows the cell voltage as a function of current density for single PEM fuel cells using a cathode prepared from Au@Pt (2:4)/C electrocatalysts and an anode prepared from Pt/C (JM) electrocatalysts. The loadings of total metals were all 0.4 mg cm^{-2}. We can see that the open-circuit potential is around 1.0 V and maximum power density is 479 mW cm^{-2} at 0.436 V.

Unfortunately, due to the fact that the maximum power density was somewhat low, it might be feasible to use such a catalyst only in a low current density range. More work is underway toward optimizing the catalytic activity with a focus on increasing the performance. Furthermore, better performance could be obtained by optimization of the MEA manufacture.

4. Conclusions

A series of core shell structure Au@Pt/C electrocatalysts were prepared by the seed-mediated growth method. The unique structure was verified by independent measurements using UV–vis, XPS and TEM. It was found that core shell Au@Pt nanoparticles could be obtained by the seed-mediated growth method using Au as the seeds. Evaluation of the Au@Pt/C catalysts for the O_2 reduction by LSV measurements revealed high ORR activity, with maximum activity being observed for the Au@Pt (2:4)/C catalyst. The ORR of Au@Pt (2:4)/C in acid solution proceeded an approximately four-electron pathway, through which oxygen was directly reduced to water. With the core shell structure, the utilization of Pt could be improved.

Acknowledgments

The authors gratefully acknowledge the financial support from the National Natural Science Foundation (No. 20703031), Doctoral Program of Higher education (No. 20070247055), Program for Young Excellent Talents in Tongji University (No. 2006KJ022), Shanghai Leading Academic Discipline Project (No. B303), and 111 Project (No. B08019).

References

[1] H.R. Colón-Mercado, B.N. Popov, J. Power Sources 155 (2006) 253.
[2] P. Gouérec, M. Savy, Electrochim. Acta 44 (1999) 2653.
[3] M. Min, J. Cho, K. Cho, H. Kim, Electrochim. Acta 45 (2000) 4211.
[4] B. Wang, J. Power Sources 152 (2005) 1.
[5] J.H. Kim, A. Ishihara, S. Mitsushima, N. Kamiya, K.I. Ota, Electrochim. Acta 52 (2007) 2492.
[6] K.C. Lee, A. Ishihara, S. Mitsushima, N. Kamiya, K.I. Ota, Electrochim. Acta 49 (2004) 3479.
[7] D.L. Wang, H.L.L. Xin, Y.C. Yu, H.S. Wang, E. Rus, D.A. Muller, H.D. Abruna, J. Am. Chem. Soc. 132 (2010) 17664.
[8] J.L. Qiao, R. Lin, B. Li, J.X. Ma, J.S. Liu, Electrochim. Acta 55 (2010) 8490.
[9] K.C. Lee, L. Zhang, J.J. Zhang, J. Power Sources 170 (2007) 291.
[10] C.V. Rao, B. Viswanathan, J. Phys. Chem. C 111 (2007) 6538.
[11] E. Claud, T. Addou, J.M. Latour, P. Aldebert, J. Appl. Electrochem. 28 (1998) 57.
[12] J.P. Collman, P.S. Wagenknecht, J.E. Hutchison, Angew. Chem. Int. Ed. 33 (1994) 1537.
[13] L. Wang, Y. Yamauchi, J. Am. Chem. Soc. 132 (2010) 13636.
[14] B. Lim, M.J. Jiang, P.H.C. Camargo, E.C. Cho, J. Tao, X.M. Lu, Y.M. Zhu, Y.N. Xia, Science 324 (2009) 1302.
[15] J.L. Zhang, M.B. Vukmirovic, Y. Xu, M. Mavrikakis, R.R. Adzic, Angew. Chem. Int. Ed. 44 (2005) 2132.
[16] J.H. Zeng, J. Yang, J.Y. Lee, W.J. Zhou, J. Phys. Chem. B 110 (2006) 24606.
[17] J.F. Moulder, W.F. Stickle, P.E. Sobol, K.D. Bomben, Handbook of X-ray Photoelectron Spectroscopy, Perkin-Elmer Corporation, Minnesota, 1992.
[18] M. Watanabe, M. Uchida, S. Motoo, J. Electroanal. Chem. 229 (1987) 395.
[19] Z. Bastl, Š. Pick, Surf. Sci. 832 (2004) 566.
[20] Y.W. Ma, H.M. Zhang, H.X. Zhong, T. Xu, H. Jin, X.Y. Geng, Catal. Commun. 11 (2010) 434.
[21] A.J. Bard, L.R. Faulkner, Electrochemical Methods, 2nd ed., Wiley & Sons, New York, 2001, p. 331.